Journal of Thermal Analysis and Calorimetry, Vol. 79 (2005) 677–683

DYNAMIC THERMAL DEGRADATION STUDIES ON AMORPHOUS CARBON THIN FILMS

Y. Q. Li[1], *L. H. Zhang*[1,2] *and H. Gong*[1*]

[1]Department of Materials Science, National University of Singapore, 119260, Singapore
[2]Seagate Technology International in Singapore, Singapore

Dynamic thermogravimetry (TG) analysis for thermal degradation kinetics were applied for amorphous carbon (a-C) thin films prepared by direct-current (DC) magnetron sputtering. The degradations generally consist release of free-bonded and weakly-bonded amorphous compositions and dissociation of highly-bonded compositions of higher graphitic orders. Using deconvolution technique for differential TG (DTG) curves, the apparent activation energy (E_a) values for these stages were obtained, which were about 101–121, 117–121, 130–144 kJ mol^{-1}. Structure characterizations before and during decompositions were analyzed and interpreted using X-ray photoelectron spectroscopy (XPS), Raman spectroscopy and evolution analysis.

Keywords: *amorphous carbon, film, kinetics, thermodynamic analysis*

Introduction

Hard amorphous carbon (a-C) films have wide applications in electrical, mechanical and biomedical areas [1–3]. The films are normally prepared by techniques like magnetron sputtering, ion-beam deposition, chemical vapor deposition and cathodic-arc deposition, in which, magnetron sputtering is one of the most widely used techniques. Most of the films can be described as an amorphous matrix dispersed with graphitic nano-domains cross-linked through sp^3 bonds [4–8]. Kinetic energy of depositing species and reactive sputtering are the primary factors affecting the thermal behavior of the a-C films. These factors affect the bonding ratio, bonding configurations and bonding energies of the film structures [7–8]. There is high interest on thermal decomposition and kinetics of a-C films.

Based on dynamic TG method, some models have been proposed for acquiring kinetic parameters of heterogeneous reactions [9–15]. The Kissinger method [9] and Ozawa method [10] are two of the typical ones used widely [15]. In this paper, we studied the thermal degradations of some sputtered a-C films based on dynamic TG and DTG methods. The obtained kinetic parameters were analyzed in correlation to evolution products and the structure properties of as-deposited films.

Experimental

Deposition of a-C films

a-C films of about 1μm thick were deposited on thin Corning glass substrates (0.15 mm thickness) using a DC magnetron sputtering system (INNOTEC D28) for TG and TG-MS study. The same films of about 30 nm thick were also deposited on Si-wafer substrate for other characterizations. Detail deposition conditions and substrate treatment method can be found from our earlier publications [7–8]. Four sputtering pressures of Ar, $0.91\cdot10^{-3}$, $3\cdot10^{-3}$, $7\cdot10^{-3}$ and $16\cdot10^{-3}$ Torr, corresponding to Ar flow rate of 17, 19, 80, 165 sccm and film deposition rate of 40, 25, 18, 12 nm min^{-1}, respectively, were employed. The obtained a-C films are denoted as Film-1, Film-3, Film-7 and Film-16, with the postfix numbers representing the sputtering pressure in $1\cdot10^{-3}$ Torr.

Film characterization

Structures of the films were characterized using X-ray photoelectron spectroscopy (XPS, Physical Electronics Quantum 2000) with 0.5 eV resolution and Raman spectroscopy (RENISHAW 1000) using 514.5 nm laser.

Dynamic TG measurements were performed at seven heating rates, 0.8, 2, 5, 10, 15, 20 and 25°C min^{-1}, using a DuPont TGA 2950 analyzer with a 0.1 μg mass sensitivity and ±1°C temperature accuracy. A film with substrate of about 20 mg was heated in a platinum pan (0.02 g) under ambient gas flow of 60 cm^3 min^{-1} for air and 100 cm^3 min^{-1} for N_2. The samples were in broken pieces. They were placed in the crucible in 2–3 pieces with no covering of one with the others.

TG-MS analysis was performed for evolving products using a TG analyzer (TA Instruments, TGA 2050) interfaced to a mass spectroscopy (MS)

* Author for correspondence: masgongh@nus.edu.sg

1388–6150/$20.00

Akadémiai Kiadó, Budapest, Hungary
Springer, Dordrecht, The Netherlands

detector (Balzer Instruments, Thermlstar) equipped with a quadruple mass filter operating in a range of 1 to 175 atomic mass units (amu). The mass spectra were captured for every 5°C increase.

Atomic force microscope (AFM, DI-nanoscopy III), nano-indentator (Nanoindenter I, Nanoinstruments), and UV-Visible spectroscopy (Shimadzu UV-1601) were used for surface roughness, nano-hardness and light absorbance (A_b) of the a-C films. The hardness values were determined from the unloading segment of a load-displacement loop. Direct allowed optical band gaps of the films were obtained from the intersect $h\nu$ value by extrapolating the linear portion of the $(h\nu\alpha_{opt})^2 \sim h\nu$ curve to the $h\nu$ axis, in which, h is the Plank constant, ν the light frequency and α_{opt} the optical coefficient defined by $\alpha_{opt}=A_b(\ln 10)/t_f$, with t_f the film thickness.

Results and discussion

As-deposited Films

Figure 1 shows the typical Raman spectra of the deposited a-C films. Table 1 summarizes the characterization results for film structures and properties. The relative sp^3/sp^2 values were determined from the XPS C1s spectrum from the area ratio of the two deconvoluted binding-energy (E_b) peaks representing sp^3 bonds (E_b: ~284.3 eV) and sp^2 bonds (E_b: ~285.1 eV), respectively [3]. In a Raman spectrum, the G-peak arises from the symmetric E_{2g} vibrations of graphite-like materials while the D-peak arises from the disordered mode of graphitic vibrations, induced by substitutional atoms, sp^3 carbon, or other impurities [16–17]. Thus the intensity of D-peak with respect to the G-peak (I_d/I_g) decreases as the graphitic grain size increases. Thus, the decrease of sp^3/sp^2 values is also correlated to increased Raman G-peak frequency and the I_d/I_g ratios [17]. A gradual Raman band broadening can be observed from Film-16 to Film-1 (Fig. 2), which suggests that the rich sp^3 bonds in Film-1 break the long-range order of the graphitic structure. From Raman and XPS measurements, the graphitization of the a-C films increases in the series: Film-1>Film-3>Film-7>Film-16. This is mainly because that the depositing carbon species at lower kinetic energy or higher sputtering pressure tend to maintain their lowest energy state that is sp^2. This also correlates to the reduced nano-hardness and optical band gaps. Increased surface roughness from Film-1 to Film-16 can be explained from the existence of entrapped or weakly-bonded species in the films, the amount of which increases with the sputtering pressure (Table 1).

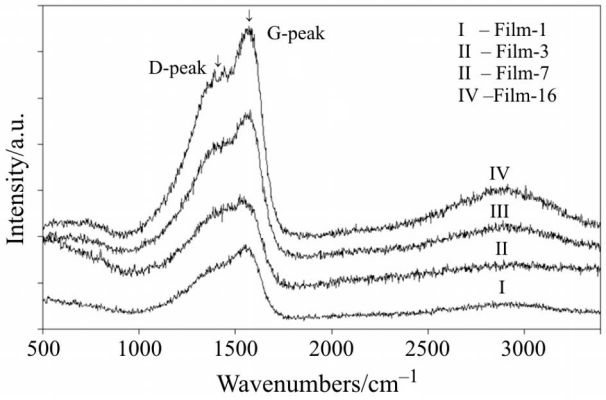

Fig. 1 Raman spectra of the as-deposited a-C films

Thermal degradation in air and N_2 atmospheres

The glass substrate after treatment showed less than 0.07% of total mass changes from the dynamic TG measurement to 650°C. Comparing to the film mass changes of ~1%, the mass change due to substrate can be neglected. Figure 2 shows some of the dynamic mass loss curves (Fig. 2a) and their first order derivatives (DTG) (Fig. 2b) for the a-C films in air atmosphere at different heating rates. The same kind of measurements in N_2 (not shown) show that the onset decomposition temperature is 100–150°C higher than those in air. Both results indicate that the onset decomposition temperature increases with the kinetic energy of carbon species prior to film deposition, or Film-16<Film-7<Film-3<Film-1. The increased amount of interstitial and weakly-bonded compositions in a-C film sputtered at higher pressure can be attributed to the lower thermal stability of the structure [7–8]. As discussed above, these structures tend to have higher graphitization or lower sp^3/sp^2 bonding ratio. The relative amount of interstitial and weakly-bonded compositions in a-C film can be revealed from DTG curves (Fig. 2b). These compositions can be released at relatively lower temperatures due to their weaker

Table 1 Some characterization parameters of the sputtered a-C films

	R_a /nm (1·1 μm)	Direct optical band gap/eV	Hardness/GPa	Raman G-peak	Raman I_d/I_g	sp^3/sp^2 ratio/ XPS
Film-1	0.245	1.20	18	1564	1.96	32.5
Film-3	0.365	0.89	16	1563	2.24	28.6
Film-7	0.393	0.83	15	1570	2.37	24.3
Film-16	0.803	0.80	13	1582	2.91	17.7

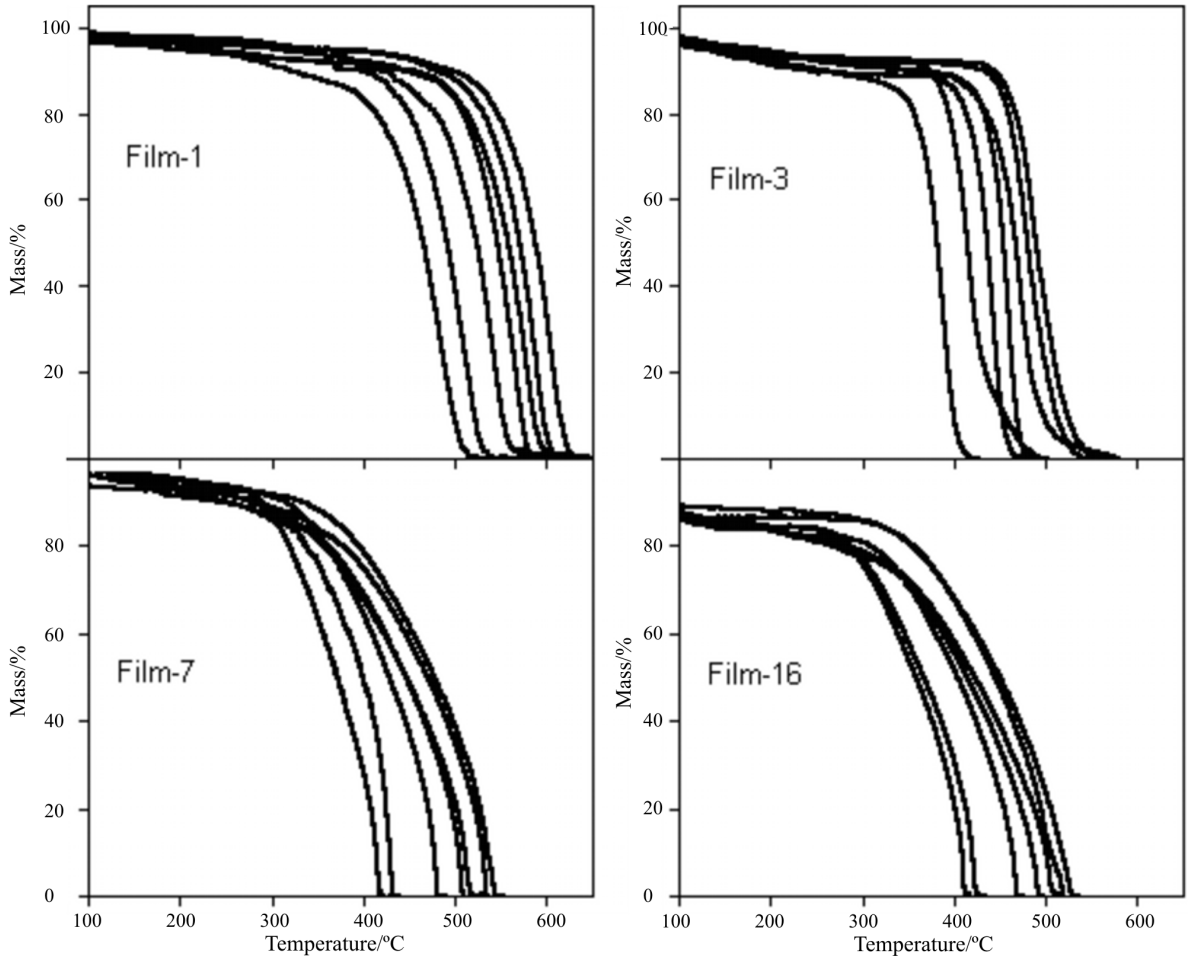

Fig. 2a Dynamic TG curves of the a-C films at heating rates of 0.8, 2, 5, 15, 20 and 25 °C min^{-1} in air

bonding with surrounding structures, yielding a broad DTG peak at lower temperatures prior to the peak for dissociation of highly-bonded graphitic carbons.

From the DTG curves in Fig. 2b, Film-1 and Film-3 show apparently single step decompositions in contrasting to the two-step ones for Film-7 and Film-16.The broad DTG humps at lower temperatures for Film-7 and Film-16 correspond to the release of interstitial and weakly-bonded molecules [7–8]. The amount of these components in Film-1 and Film-3 might be too small to be visualized in the experiment. The results suggest that as the sputtering pressure increases the film structures become more weakly-bonded or have lower bonding integrity, leading to multiple decomposition steps in dynamic TG analysis. Comparing the TG and DTG results in air and in N_2, the broad DTG hump at lower temperatures corresponding to decomposition of interstitial and weakly-bonded compositions in air (Fig. 2b) is comparatively insignificant in N_2 (not shown). The results suggest that decomposition of the interstitial and weakly-bonded components are mainly due to oxidation.

TG-MS analysis was applied to characterize the evolved products of the a-C films during thermal decompositions. Typically, oxidation components such as CO_2 and H_2O were seen in almost the full range heating in either air or N_2 environment. At lower temperatures (<450°C), all the evolved components are small fractions with m/e less than 50. Heavy components with m/e of 73, 114, 117 appeared when the temperature reached ~550– 600°C. These heavy components are highly possible the fractions with graphitic ring structures that have higher bonding ratio and give heavier species once split.

From Fig. 2b, as the heating rate (q) increases from 0.8 to 25°C, the widths of DTG peaks reduces for Film-1 but increases for the rest three films. Generally, the DTG peak narrows at higher heating rates because the reaction tends to be faster at higher temperatures [18]. The gradual broadening of the DTG peaks at higher heating rates for Film-3 to Film-16 might be due to the structure graphitization at lower heating rates, resulting in more consolidated structures. The graphitization could be carried out easily for the films with higher amount of pre-existing sp^2 graphite nano-crystals. Graphitization of the a-C films after heating can be observed from the Raman

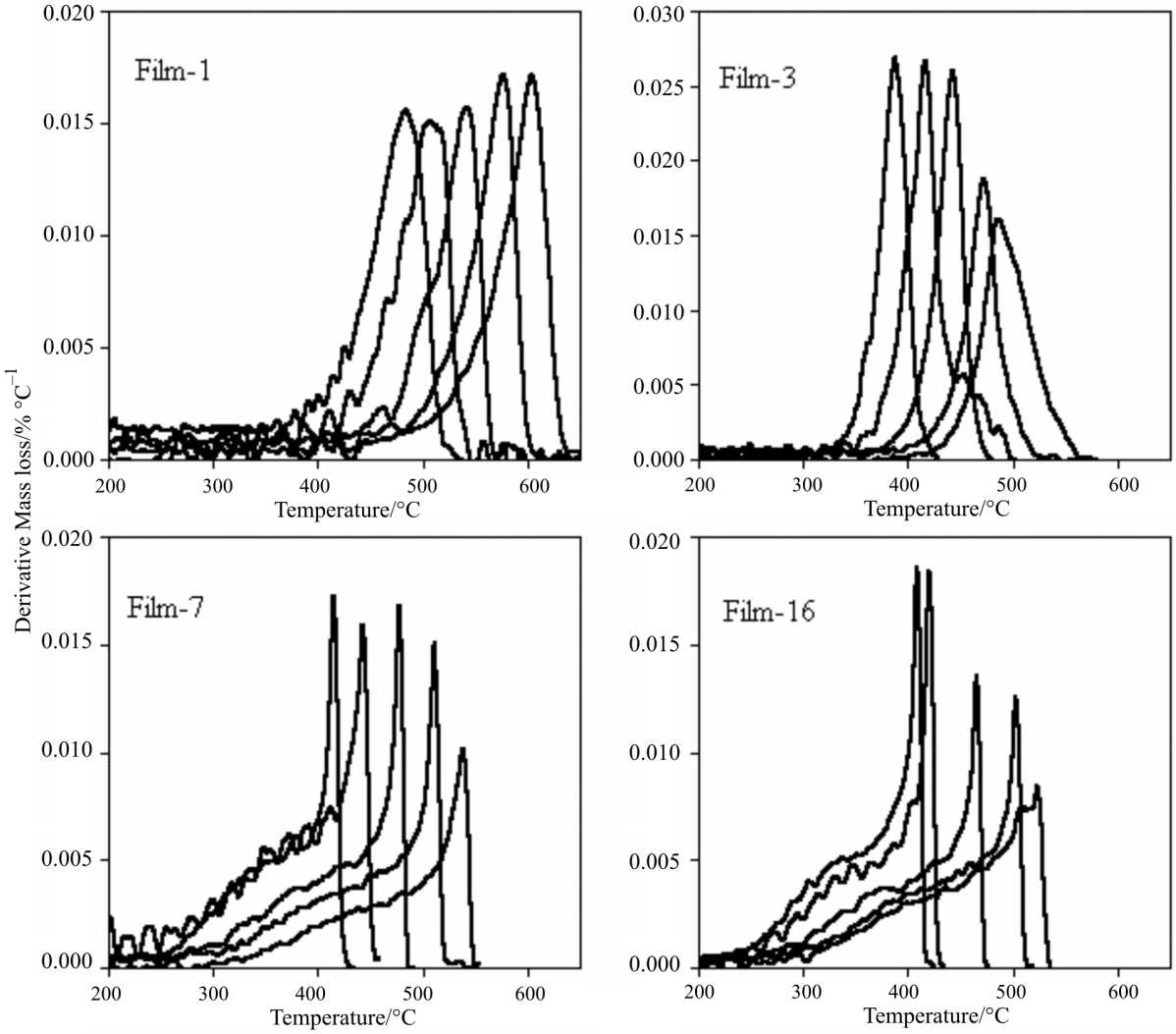

Fig. 2b Dynamic DTG curves of the a-C films at heating rates of 0.8, 2, 5, 15, 20 and 25°C min^{-1} in air

results (not shown) for better resolved G-peak and D-peak and moving of G-peak to higher frequencies.

Thermal degradation kinetics

The kinetics of heterogeneous decompositions is traditionally described by the basic equation:

$$\frac{d\alpha}{dt} = k(T)f(\alpha) \qquad (1)$$

where α represents the extent of reaction (α=0~1), t is the reaction time, $k(T)$ the rate constant related to temperature T, and $f(\alpha)$ the mathematical expression describing the dependence of the reaction rate with the extent of reaction. In most cases the temperature dependence of $k(T)$ can be satisfactorily described by the Arrhenius equation $k = k\mathrm{e}^{-E_a/RT}$ [19]. Its substitution into Eq. (1) yields

$$\frac{d\alpha}{dt} = A\exp\left(\frac{-E_a}{RT}\right)f(\alpha) \qquad (2)$$

where E_a is the activation energy and A the pre-exponential factor.

To calculate E_a from dynamic TG results, the Kissinger [9] method, which is based on a series of T_{max} values, is used. Since the maximum rate occurs when da/dt=0, from Eq. (1) at $f(\alpha)=(1-\alpha)^n$ (n^{th} order reaction), we obtain [10]:

$$\left(\frac{\mathrm{d}^2\alpha}{\mathrm{d}T^2}\right)_{max} = 0 = \left(\frac{\mathrm{d}\alpha}{\mathrm{d}T}\right)_{max}\left[\frac{E_a}{RT_{max}^2} - \frac{A}{q}\exp\left(\frac{-E_a}{RT_{max}}\right)n(1-\alpha)_{max}^{n-1}\right] \qquad (3)$$

where q is the heating rate, R the molar gas constant. Kissinger has shown that $n(1-\alpha_{max}^{n-1}) = 1$ for different heating rates. The logarithm expression of Eq. (3) is:

$$\ln\left(\frac{q}{T_{max}^2}\right) = -\frac{E_a}{R}\left(\frac{1}{T_{max}}\right) \quad (4)$$

The slope of $\ln(q / T_{max}^2)$ *vs.* $1/T$ has a slope of $-E_a/R$.

Ozawa [10] can further deduce the rate of mass loss by the equation:

$$\frac{d\alpha}{dT} = \frac{A}{q}\exp\left(\frac{-E_a}{RT}\right)g(\alpha) \; or \; g(\alpha) = \int_0^{\infty}\frac{d\alpha}{(1-\alpha)^n} = \frac{A}{q}\int_0^{T}\exp\left(\frac{-E_a}{RT}\right)dT = \frac{AE_a}{qR}\,p(x) \quad (5)$$

The logarithmic function of Eq. (5) gives:

$$\log g(\alpha) - \log p(x) = \log\frac{AE_a}{qR} \quad (6)$$

$\log(AE_a/qR)$ is independent of temperature even though $\log[g(\alpha)]$ and $\log[p(x)]$ contain T. To a first approximation $\log[p(x)]$ is a linear function of $1/T_\alpha$ if x is sufficiently high, and $\log[g(\alpha)]$ *vs.* $1/T_\alpha$ should be linear. The Ozawa method is based on the following expression,

$$\log g(\alpha) \cong \log\frac{AE_a}{R} - \log q + \log p\left(\frac{E}{RT}\right) \quad (7)$$

Using Doyle's approximation for expressions of $\log[p(E_a/RT)]$ in the case of $20<E_a/RT<60$ and mathematical expressions for $\log[g(\alpha)]$ and $\log[p(x)]$, Eq. (8) can be obtained by differentiating Eq. (7) at constant conversion yields

$$E_a = \frac{R}{0.457}\frac{\log\left(\frac{q_1}{q_2}\right)}{\left(\frac{1}{T_1}-\frac{1}{T_2}\right)} \quad (8)$$

The apparent activation energy E_a can be obtained from the Ozawa method by plotting $\log(q)$ *vs.* $1/T$ for α constants.

The Kissinger method needs a series T_{max} values. These values can be obtained from the highest DTG peaks (Fig. 2b). For Film-1 and Film-3, there is only one apparent DTG peak and the T_{max} values are easily obtained. For Film-7 and Film-16, the DTG curves can be deconvoluted into multiple peaks representing different reactions. Therefore, the T_{max} values for the specific reactions can be used for kinetic analysis based on the Kissinger method. Using curve-fitting technique, each DTG curve for Film-7 and Film-16 can be best deconvoluted into three Gaussian fits. Figure 3 shows the typical fitting results. DTG-1, DTG-2 and DTG-3 represent the release of free-bonded compositions, weakly-bonded compositions and highly-bonded graphitic compositions, respectively. The assignments of these peaks are based on the discussions above on TG and TG-MS data.

Kissinger method is simple. It yields average E_a values for different reaction steps that is not available using the Ozawa method. However, Ozawa method allows calculating E_a values with the progress of reaction, which is very important in interpreting reaction mechanisms [9–10]. Figure 4 shows the Kissinger $\ln(q/T_{max}^2)$ *vs.* $1/T$ plots for the highly-bonded structures for the four a-C films. For Film-7 and Film-16, the T_{max} values were obtained from the DTG-3 (Fig. 3). Therefore, the E_a values obtained from the plots in Fig. 4 represent the decomposition of the highly-bonded structures in the a-C films. The very good linear correlations (r^2=~0.99) of the plots in Fig. 5 suggest good applicability of the Kissinger method to the thermal decomposition of the a-C films. For Film-7 and Film-16, the T_{max} values obtained from DTG-1 and DTG-2 (Fig. 3) for the release of free-bonded and weakly-bonded compositions also yielded good application of Kissinger method (r^2 >0.97). The E_a values obtained from the Kissinger plots are listed in Table 2. The E_a value corresponding to the decomposition of bonded structure is the highest for Film-1 but close for the rest three films. However, those corresponding to the release of free and weakly-bonded compositions are significantly less than those for the bonded structure. The results also indicate that the films become less stable in air due to the oxidation effect that reduces the energy barrier for the decomposition.

The Ozawa method allows the analysis of E_a in the process of reaction. Typical plots of $\log(q)$ *vs.* $1/T$ as a function of conversion are shown in Fig. 5 for Film-1. The calculated E_a values following Eq. (8) are summarized in Table 3. The results show that as the reaction progressed, E_a gradual reduces for Film-1 and Film-3 but increases for Film-7 and Film-16. For

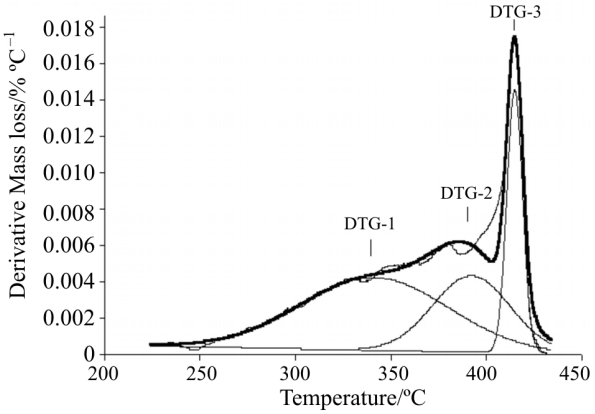

Fig. 3 A typical DTG curve (Film-7, at 0.8°C min^{-1} in air) that is resolved into three Gaussian fits representing the decompositions due to removal of unbonded (DTG-1), loosely-bonded (DTG-2) and bonded compositions (DTG-3) in the a-C film

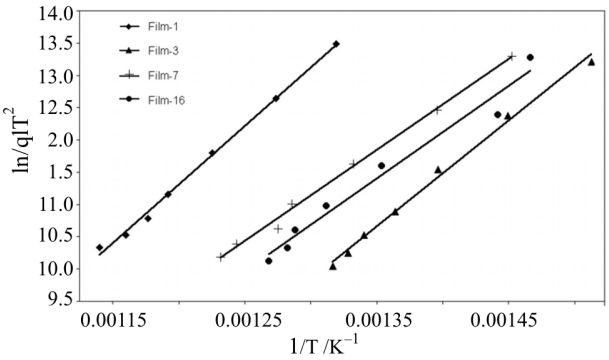

Fig. 4 Kissinger plots for the bonded structure decomposition of the a-C films in air

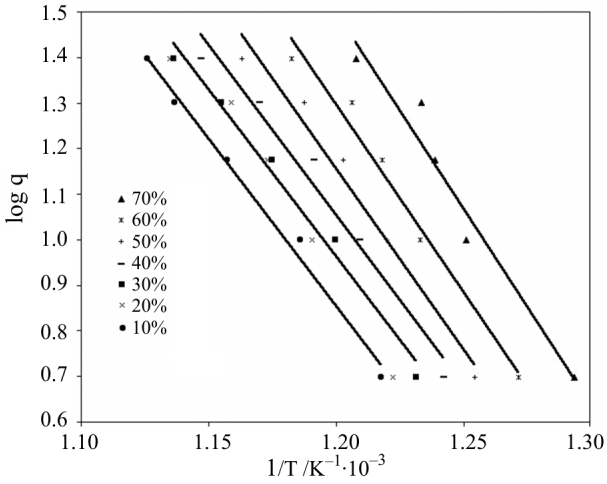

Fig. 5 Typical Ozawa plots of Film-1 in dynamic air atmospheric TG measurements

Film-1 and Film-3, this indicates gradual less stable structures as the reaction progresses, for Film-7 and Film-16, this might be due to the release of large amount of free-bonded and weakly-bonded compositions at early reactions.

Conclusions

The degradations of a-C films generally consisted of dissociations of free-bonded, weakly-bonded amorphous compositions and graphitic structures. Using Kissinger method and deconvolution technique for DTG curves, the apparent activation energy (E_a) values for could be obtained for the stages, which were about 101–108, 117–121 and 130–144 kJ mol^{-1}, respectively. Release of free-bonded and weakly-bonded compositions was accelerated by oxidation. The difference in activation energy can be interpreted from structure sp^3/sp^2 bonding ratios. The films with higher structure ordering and bonding ratio (Film-1 and Film-3) showed reduced E_a with the progress of reactions while those with larger amount of free-bonded and weakly-bonded compositions (Film-7 and Film-16) had E_a increased.

Table 2 Apparent activation energy E_a (kJ mol^{-1}) values obtained from Kissinger method

	Air						N_2	
	Free-bonded		Weakly-bonded		Bonded		Bonded	
	E_a	r^2	E_a	r^2	E_a	r^2	E_a	r^2
Film-1		–		–	144	0.99		–
Film-3		–		–	137	0.99	147	0.93
Film-7	108	0.98	117	0.99	131	0.99	136	0.93
Film-16	101	0.98	121	0.98	130	0.97	134	0.96

Table 3 Change of apparent activation energies (E_a) with extent of reaction in air calculated by Ozawa method

α*	E_a/kJ mol^{-1}			
	Film-1	Film-3	Film-7	Film-16
70	156.1	126.5	108.9	–
60	149.9	129.8	119.3	105.4
50	144.8	128.4	124.5	118.5
40	135.8	122.5	128.8	131.3
30	133.2	114.5	130.6	140.2
20	132.5	106.3	132.2	143.6
10	131.7	96.2	129.0	140.0

*α represented the mass% of the residue film during TG measurements

References

1 B. Bhushan, Diamond Relat. Mater., 8 (1999) 1985.
2 A. Schenk, B. Winter, J. Biener, C. Lutterloh, U. A. Schubert and J. Kupper, J. Appl. Phys., 77 (1995) 2462.
3 J. Robertson, Mater. Sci. Eng., R37 (2002) 129.
4 D. Tanaka, S. Ohshio and H. Saitoh, Jpn. J. Appl. Phys., 39 (2000) 6008.
5 S. Anders, J. Diaz, J. W. Ager lll, R. Y. Lo and D. B. Bogy, Appl. Phys. Lett., 71 (1997) 3367.
6 L. H. Zhang, H. Gong and J. P. Wang, J. Appl. Phys., 91 (2002) 9646.
7 L. H. Zhang, H. Gong and J. P. Wang, J. Phys.: Condens. Matter, 14 (2002) 1697.
8 X. Xiao, W. Jiang, L. Song, J. Tian and X. Hu, Chem. Phys. Lett., 310 (1999) 240.
9 A. Mianowski, J. Therm. Anal. Cal., 74 (2003) 953.
10 N. Régnier and S. Fontaine, J. Therm. Anal. Cal., 64 (2001) 789.
11 D. W. Van Krevellen, C. van Herden and F. J. Huntjens, Fuel, 30 (1951) 253.
12 H. H. Horowitz and G. Metzger, Anal. Chem., 35 (1963) 1464.
13 A. W. Coats and J. P. Redfern, J. Polym. Sci. Polym. Lett., Ed., 3 (1965) 917.
14 J. R. MacCallum and J. Tanner, Europ. Polym. J., 6 (1970) 1033.
15 N. Regnier and C. Guibe, Polym. Degrad. Stab., 55 (1997) 165.
16 R. O. Dillon and J. A. Woollam, Phys. Rev., 29 (1984) 3482.
17 M. Yoshikawa, Mater. Sci. Forum, 52–53 (1989) 365.
18 T. Hatakeyama and Z. Liu, Handbook of Thermal Analysis, J. Wiley & Sons, New York 1998.
19 O. Levenspiel, Chemical Reaction Engineering: An Introduction to the Design of Chemical Reactors, Wiley, New York 1999.

Received: October 31, 2003
In revised form: September 15, 2004